

## Influence of MgO on the Electrochemical Performance of Nickel Electrode in Alkaline Aqueous Electrolyte

B. Shruthi<sup>1</sup>, B. J. Madhu<sup>2,\*</sup>, V. Bheema Raju<sup>3</sup>, S. Vynathey<sup>4</sup> and B. Veena Devi<sup>1</sup>

<sup>1</sup>Department of Chemistry, Dr. Ambedkar Institute of Technology, Bangalore - 560 056, India

<sup>2</sup>Post Graduate Department of Physics, Government Science College, Chitradurga- 577 501, India

<sup>3</sup>Department of Chemistry, Dayananda sagar College of Engineering, Bangalore - 560 078, India

<sup>4</sup>Materials Technology Division, Central Power Research Institute, Bangalore- 560 080, India

Received: June 07, 2016, Accepted: July 25, 2016, Available online: September 08, 2016

**Abstract:**  $\beta$ -nickel hydroxide ( $\beta$ -Ni(OH)<sub>2</sub>) was prepared using precipitation method. Magnesium oxide (MgO) was synthesized by solution combustion method using magnesium nitrate as oxidizer and urea as a fuel. The effects of MgO additive on the structure and electrochemical performance of  $\beta$ -Ni(OH)<sub>2</sub> electrode are examined. The structure and property of the MgO added  $\beta$ -Ni(OH)<sub>2</sub> were characterized by X-ray diffraction (XRD), thermal gravimetric-differential thermal analysis (TG-DTA), Scanning electron microscopy (SEM), and Energy Dispersive X-ray (EDX) analysis. The results of the TG-DTA studies indicate that the MgO added  $\beta$ -Ni(OH)<sub>2</sub> contains adsorbed water molecules and anions. Partial substitution of MgO for graphite to  $\beta$ -nickel hydroxide is found to exhibit improvement in the electrochemical activity. Anodic peak potential ( $E_{pa}$ ) and cathodic peak potential ( $E_{pc}$ ) values are found to decrease remarkably after the incorporation of MgO into the  $\beta$ -Ni(OH)<sub>2</sub> electrode. Further, addition of MgO is found to enhance the reversibility of the electrode reaction. Compared with  $\beta$ -Ni(OH)<sub>2</sub> electrode, MgO substituted  $\beta$ -Ni(OH)<sub>2</sub> electrode is found to exhibit higher proton diffusion coefficient. These findings suggest that the MgO substituted  $\beta$ -Ni(OH)<sub>2</sub> electrode possess improved electrochemical properties such as enhanced reversibility of electrode reaction and higher proton diffusion coefficient and thus can be recognized as a promising candidate for the battery electrode applications.

**Keywords:** Nickel hydroxide; MgO additive; Electrode material; Electrochemical properties; Proton diffusion coefficient

### 1. INTRODUCTION

Recently, increasing power demands for hybrid electric vehicles and power tools have forced researchers to look for highly effective battery devices to store electrical energy. In the recent decades, much interest has concentrated on the development of novel electrode materials for advanced energy conversion and storage devices [1-3]. Among numerous active electrode materials, nickel hydroxide (Ni(OH)<sub>2</sub>) is the most promising candidate and it is widely used in rechargeable nickel-based batteries as a positive electrode material due to its high stability in alkaline electrolyte and thermal stability [4,5]. In recent times, pasted nickel electrodes have been significantly developed to meet the requirement of high capacity in secondary batteries such as Ni-Cd, Ni-Fe, Ni-Zn and

Ni-MH due to their simple fabrication and high incorporation of active materials. However, the pasted nickel electrodes are found to exhibit low active material utilization due to the poor conductivity of the Ni(OH)<sub>2</sub> powder. To overcome this drawback, the preparation of a high performance nickel electrode becomes significant and essential. These objectives could be achieved by selecting the proper conditions for the synthesis of high performance active material by using suitable additives that could provide the conductive network to enhance the utilization of the nickel hydroxide. It has been found that the reversibility of the Ni(II)/Ni(III) electrochemical reaction could be increased by the incorporation of suitable additives. [6-8].

The nickel hydroxide (Ni(OH)<sub>2</sub>) is found to exist in two polymorphic forms, namely  $\alpha$ -Ni(OH)<sub>2</sub> and  $\beta$ -Ni(OH)<sub>2</sub>, which are transformed into  $\gamma$ -NiOOH and  $\beta$ -NiOOH, respectively during

\*To whom correspondence should be addressed: Email: bjmadhu@gmail.com  
Phone: 08194234270

charging [9-12]. The  $\beta$ -phase exhibits superior stability compared to the  $\alpha$ -Ni(OH)<sub>2</sub>. The  $\beta$ -Ni(OH)<sub>2</sub> is normally oxidized to  $\beta$ -NiOOH in a charge process. The electrochemical performance of the  $\beta$ -Ni(OH)<sub>2</sub> is known to be affected by its size and morphology. It has been found that  $\beta$ -Ni(OH)<sub>2</sub> with a smaller crystalline size and enhanced specific surface area exhibits better electrochemical properties [7]. Several studies have revealed that incorporation of metallic compounds into the nickel electrode is an effective approach to improve electric conductivity of the active material and to give rigidity to the structure to minimize volume changes produced during cycling [13-17]. Moreover, adding metallic compounds such as Co(OH)<sub>2</sub>, CuO, CdO, Zn(OH)<sub>2</sub> and ZnO into the nickel electrode are reported to have beneficial effects such as inhibiting the swelling of the nickel electrode during charging and thus prolong the cycle-life of rechargeable batteries [5, 18-21].

In this study, the influence of Magnesium oxide (MgO) on the structural, thermal and electrochemical properties of the nickel hydroxide electrodes was investigated and the results are reported.

## 2. EXPERIMENTAL

### 2.1. Synthesis of $\beta$ -nickel hydroxide

The chemical synthesis of  $\beta$ -nickel hydroxide was attained in three steps viz. (i) addition of the reagents, (ii) digestion of the precipitate and (iii) drying and grinding of the precipitate. Analar grade potassium hydroxide (KOH) and nickel sulphate (NiSO<sub>4</sub>) were used as reagents. Triple distilled water was used for the solution preparation and washing of the precipitate. A solution of 1 M KOH was added to 1 M NiSO<sub>4</sub> solution by dripping at a flow rate of 10 ml min<sup>-1</sup> with continuous stirring. The addition of the reagent was ended when the pH of the suspension attains 13. Then the mixture was permitted to stand for 24 h for digestion of the precipitate. The separation of the precipitate from the excess reagent was done by centrifugation at 1500 rpm for 1 h. The precipitate was washed thoroughly with the distilled water. Barium chloride (BaCl<sub>2</sub> (1 M)) in excess was added to wash water, causing precipitation of barium sulphate (BaSO<sub>4</sub>). The washing of the precipitate was terminated when the white precipitate of BaSO<sub>4</sub> was no more found in the wash water. This nickel hydroxide precipitate was dried at 60 °C for 48 h.

### 2.2. Preparation of Magnesium oxide

Magnesium oxide (MgO) was prepared by solution combustion method using stoichiometric composition of magnesium nitrate as oxidizer and urea as a fuel. The aqueous solution containing redox mixture was taken in a pyrex dish and heated in a muffle furnace maintained at 500 ± 10 °C. The mixture finally yields porous and voluminous powder.

### 2.3. Preparation of nickel hydroxide electrodes

In the present work, the following two compositions of the electrode materials were attained viz. (i) with no additives (pure  $\beta$ -Ni(OH)<sub>2</sub> electrode) : 85 %  $\beta$ -Ni(OH)<sub>2</sub>, 10 % graphite and 5 % polytetrafluoroethylene (PTFE) as binder and (ii) with MgO additive : 85 %  $\beta$ -Ni(OH)<sub>2</sub>, 5% graphite, 5% MgO and 5% PTFE as binder. Similar compositions have been suggested by others [8, 21-23]. The test electrode was made by first mixing the prepared sample nickel hydroxide powder with graphite powder and PTFE solution in the form of slurry. The resulting slurry was pasted onto a

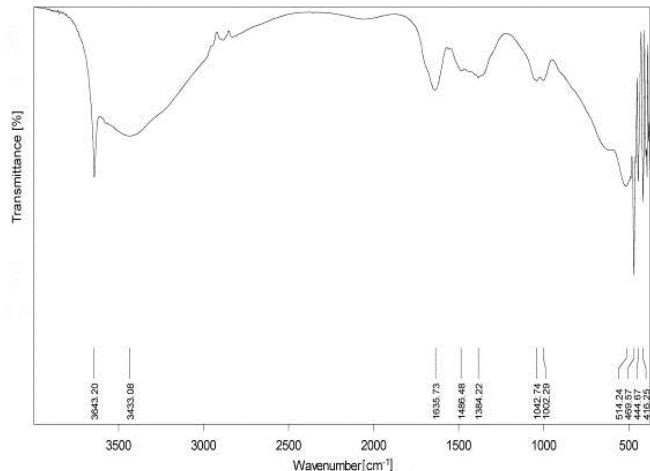


Figure 1. FTIR spectrum of  $\beta$ -Ni(OH)<sub>2</sub>.

nickel sheet. After being coated with the paste, the resulting electrode was dried at 80 °C for 1 hr. The backside of the electrode and the wire were insulated with Teflon tape. The electrodes have the following dimensions: 1cm × 1cm area.

### 2.4. Characterization

The FT-IR (Infra-red) spectrum (400-4000 cm<sup>-1</sup>) of the nickel hydroxide was recorded on a Bruker Alpha spectrophotometer in KBr pellets. Structure of the fabricated MgO added  $\beta$ -Ni(OH)<sub>2</sub> electrode was determined using X-ray diffraction analysis, with a CuK $\alpha$  radiation source ( $\lambda = 1.4581 \text{ \AA}$ ). Thermal gravimetric-differential thermal analysis (TG-DTA) of MgO added  $\beta$ -Ni(OH)<sub>2</sub> electrode was carried out by Perkin Elmer STA 6000 thermal analyzer. Morphological and composition studies of MgO added  $\beta$ -Ni(OH)<sub>2</sub> electrode were carried out using Scanning Electron Microscope (SEM) attached with Energy Dispersive X-ray (EDX) Analyzer (Model: Leica S440i INCA X-sight).

### 2.5. Electrochemical measurement

Cyclic voltammetry (CV) measurements were carried out using CHI604D electrochemical workstation. For CV studies, the test electrode prepared as described above was used as a working electrode. The platinum foil was used as a counter electrode; Ag/AgCl electrode was used as a reference electrode and 6M KOH solution was used as an electrolyte. Prior to CV studies the electrodes were activated in 6M KOH solution. After resting for 30 min in the KOH solution, the cyclic voltammograms (CVs) were obtained. The cyclic voltammograms (CVs) were recorded in the potential range between -1 and +1V vs. Ag/AgCl at various scan rates and current responses were measured. All measurements were carried out at room temperature.

## 3. RESULTS AND DISCUSSION

Fig. 1 shows the FT-IR spectrum of the as-prepared nickel hydroxide. The FT-IR spectrum confirms that the prepared nickel hydroxide can be characterized as  $\beta$  form, due to the existence of (i) a narrow and strong band at 3643 cm<sup>-1</sup> relating to the  $\nu(\text{OH})$  stretching vibration, which indicates hydroxyl (OH) groups in a

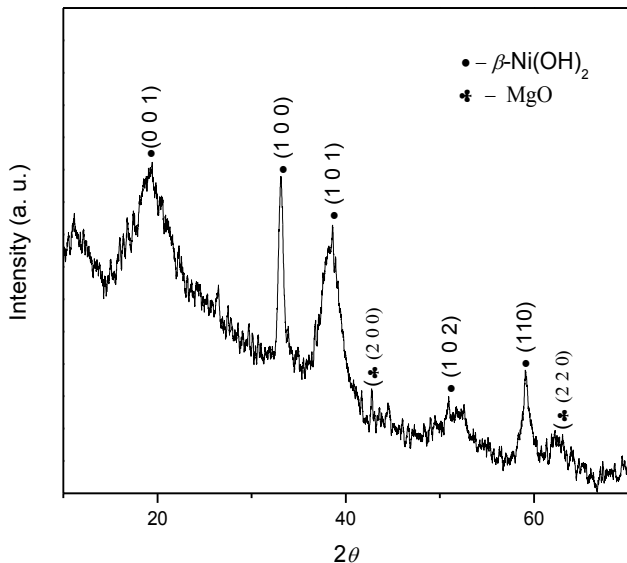


Figure 2. XRD pattern of MgO added  $\beta$ -Ni(OH)<sub>2</sub> electrode material.

free configuration, (ii) the strong narrow band at 514 cm<sup>-1</sup> corresponding to vNi-OH vibration, and (iii) a band around 469 cm<sup>-1</sup> resulting from the Ni-O stretching lattice vibration mode, v(Ni-O) [22, 24–28]. The peak observed at 1635 cm<sup>-1</sup> generally ascribed to water molecules adsorbed on the surface of the particles. This surface water is believed to improve the nickel hydroxide particles wettability [29], thus resulting in an enhanced proton transport within the active material during the charge/discharge process, and thereby a better utilization of the electrode material.

Fig. 2 represents the XRD pattern of the MgO added  $\beta$ -nickel hydroxide. Analysis of X-ray diffraction pattern revealed the presence of cubic phase of MgO with face-centered lattice within the electrode material (JCPDS card 78-0430). The diffraction peaks observed at around 19°, 33°, 38.5°, 52° and 59° are indexed entirely to a (space group: P3m1) crystal phase of  $\beta$ -Ni(OH)<sub>2</sub>, with the lattice constants of  $a = 3.130 \text{ \AA}$  and  $c = 4.630 \text{ \AA}$ , which are well matched with the reported standard values (JCPDS card 74-2075). No other peaks for the impurities such as  $\alpha$ -Ni(OH)<sub>2</sub> or other phases are noticed in the pattern. This indicates that pure  $\beta$ -Ni(OH)<sub>2</sub> was obtained under the present synthetic conditions. All of the diffraction peaks are broad, indicating the nanoscale dimensionality of the crystallites [22, 30]. In general, the broadening of XRD peaks may result from small grain sizes or structural micro distortions in the crystal. It has been observed that anomalous broadening of the (1 0  $l$ ) reflection lines ( $l \neq 0$ ) cannot be ascribed to crystallite size alone. Whereas, structural defects such as stacking faults and/or proton vacancies also play a significant role in explaining this broadening [17, 19]. The (1 0 1) line displays a relationship with electrochemical activity, probably due to the presence of stacking faults in the crystalline lattice of the synthesized nickel hydroxide powders [23, 31, 32]. It is known that the activity of nickel hydroxide is associated with its crystal structure [33]. The more disordered the crystal, the higher the activity. Structural disorder in nickel hydroxide can provide a better path for the

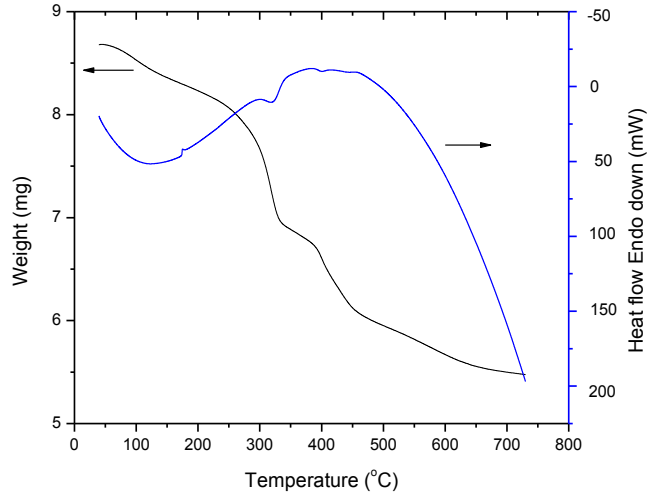


Figure 3. TG and DTA curves of the MgO added  $\beta$ -Ni(OH)<sub>2</sub> electrode material.

diffusion of protons within the NiO layers and can help lower the free energy by increasing the entropy contribution, which can in turn increase the electrochemical reaction rate [34].

Thermal behavior of the MgO added  $\beta$ -Ni(OH)<sub>2</sub> electrode material bonded with PTFE was studied by TG-DTA analysis. Typical TG-DTA curve of the MgO added  $\beta$ -Ni(OH)<sub>2</sub> electrode material is displayed in the Fig. 3. The electrode sample underwent a three-step weight loss due to dehydration, decomposition and removal of intercalated anions along with the thermal decomposition of PTFE. The three endothermic peaks at 122.6 °C, 318.2 °C and 400.77 °C on the DTA curve are indicative of three successive stages of physico-chemical changes during the heat treatment. The first region is below 200 °C, which is related to the evaporation of the adsorbed and intercalated water molecules associated with the Ni(OH)<sub>2</sub>·X<sub>ads</sub>H<sub>2</sub>O deposit. The amount of water plays an vital role in the crystal structure and the electrochemical properties of Ni(OH)<sub>2</sub>. The TG curve shows a weight loss of 5.12 wt.% corresponding to dehydration reaction:



In the present studies, the second region is between 200 °C and 350 °C, where the samples decompose to NiO (Eq. (2)). It has been reported that decomposition of Ni(OH)<sub>2</sub> into NiO occurs between 200 °C and 350 °C [35–39]. Thus the endothermic peak with the maximum located at around 318.2 °C corresponds to the endothermic behavior of MgO added  $\beta$ -Ni(OH)<sub>2</sub> during the decomposition into NiO. This peak is related to the loss of water produced by dehydroxylation of the hydroxide layers:



The theoretical weight loss corresponding to the decomposition reaction (Eq. (2)) is 19.43%, and the practical weight loss corresponding to this reaction, estimated from the second weight loss steps of TG curve is 16.37 wt.%. The difference between the practical and theoretical weight loss may be ascribed to the presence of SO<sub>4</sub><sup>2-</sup> and intercalated anions in these materials. The third region

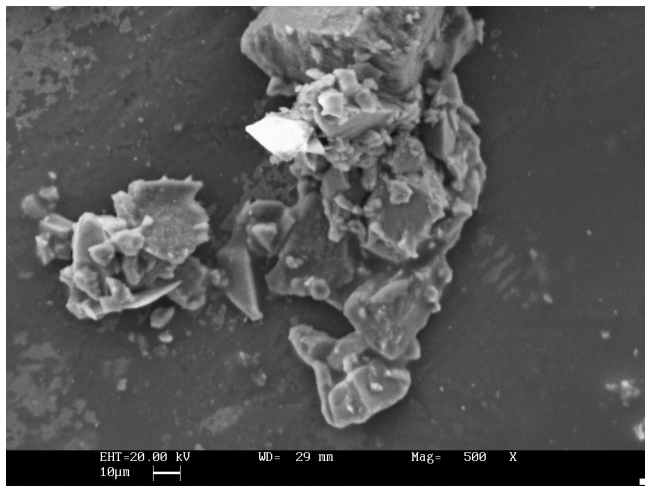


Figure 4. SEM image of MgO added  $\beta$ -Ni(OH)<sub>2</sub> electrode.

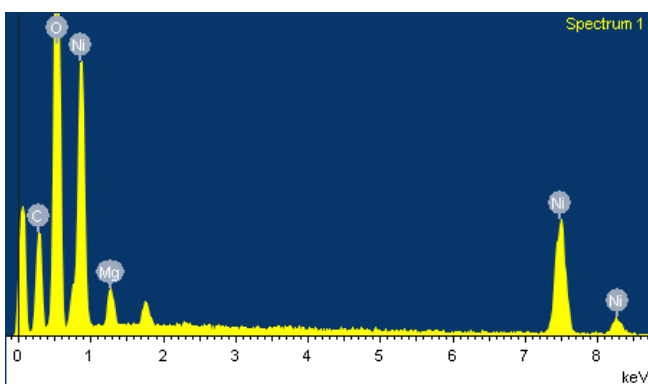


Figure 5. EDX spectrum of MgO added  $\beta$ -Ni(OH)<sub>2</sub> electrode.

between 350 °C and 600 °C can be attributed to the loss of intercalated anions and thermal decomposition of PTFE used as a binder for the preparation of electrode. The weight loss corresponding to this region is 17.64 wt.%. Above 600 °C, no appreciable weight change is observed in TG and DTA curves.

The TG analysis shows that the MgO added  $\beta$ -Ni(OH)<sub>2</sub> electrode material has considerable amount of adsorbed/intercalated water molecules, which is in agreement with the results of IR spectrum as discussed above. These water molecules may play substantial role in the enhancement of the rate-capacity performance of the electrodes because they provide the passage of proton diffusion along the molecular chain between the layers [40].

The microstructural observations have been performed on MgO added  $\beta$ -Ni(OH)<sub>2</sub> electrode using Scanning Electron Microscope (SEM). SEM image (Fig. 4) shows that  $\beta$ -Ni(OH)<sub>2</sub> electrode material is flaky and appears as aggregates of irregular tabular shapes, similar to the ball milled powders [41]. In contrast to the typical spherical particles of  $\beta$ -Ni(OH)<sub>2</sub> [7,42], it is well-known that the nickel hydroxide powders with irregular tabular shapes have a higher specific surface area that can provide a high density of active sites and thereby promote intimate interaction between the active material and the surrounding electrolyte [43,44]. Further,

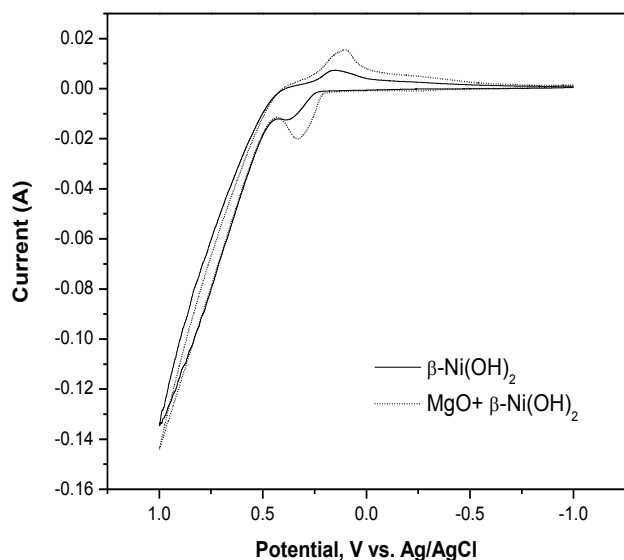
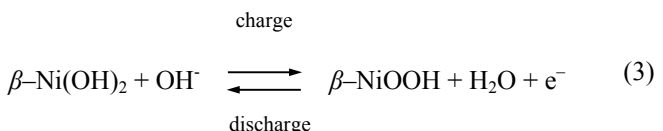


Figure 6. Cyclic voltammograms of the  $\beta$ -Ni(OH)<sub>2</sub> electrode and MgO added  $\beta$ -Ni(OH)<sub>2</sub> electrode at 0.5Vs<sup>-1</sup> scan rate.

Fig. 5 displays the EDX pattern of the MgO added  $\beta$ -Ni(OH)<sub>2</sub> electrode material. The EDX pattern shows the presence of 49.42 wt.% of Ni, 17.65 wt.% of O, 6.35 wt.% of Mg and 26.58 wt.% of C within the MgO added  $\beta$ -Ni(OH)<sub>2</sub> electrode material.

The capacitive behavior of an electrode material is generally characterized using CV curves. Fig. 6 presents typical cyclic voltammograms of the nickel electrodes using pure  $\beta$ -Ni(OH)<sub>2</sub> sample and MgO added  $\beta$ -Ni(OH)<sub>2</sub> electrode material in 6M KOH electrolyte at the scan rate of 0.5Vs<sup>-1</sup> at the potential window of -1 – +1V vs. Ag/AgCl. For both pure  $\beta$ -Ni(OH)<sub>2</sub> electrode and MgO added  $\beta$ -Ni(OH)<sub>2</sub> electrode, at a scan rate of 0.5Vs<sup>-1</sup>, one anodic nickel hydroxide oxidation peak and one cathodic oxyhydroxide reduction peak are noticeable on the CV curves. For electric double-layer capacitors, CV curves appear nearly rectangular; however, for faradaic redox reactions, large redox current peaks are present. Our results thus indicate that the observed pair of strong redox peaks are mainly due to the Faradaic redox reactions. For the  $\beta$ -Ni(OH)<sub>2</sub> electrode material, the surface faradic reactions will proceed as [24],



The anodic peak is due to the oxidation of the  $\beta$ -Ni(OH)<sub>2</sub> to  $\beta$ -NiOOH and the cathodic peak is due to the reverse process. Quasi-reversible electron transfer process is visible in the CV curve, indicating that the capacitance is primarily based on redox mechanism [12].

In order to compare the characteristics of the two electrodes, CV data in Fig. 6 consisting of anodic nickel hydroxide oxidation peak and cathodic oxyhydroxide reduction peak potentials is tabulated in Table 1. Normally, the average of the anodic and cathodic peak potentials ( $E_{\text{rev}}$ ) can be taken as an estimate of the reversible poten-

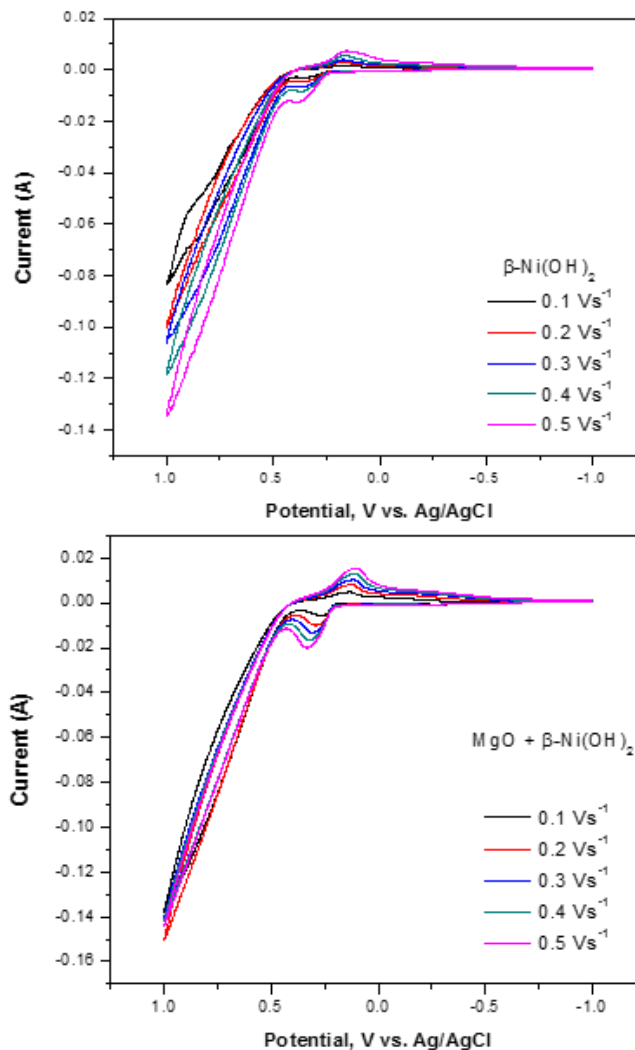


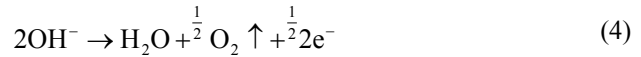
Figure 7. Cyclic voltammograms of the pure  $\beta$ -Ni(OH)<sub>2</sub> electrode and MgO added  $\beta$ -Ni(OH)<sub>2</sub> electrode at various scan rates.

tial for nickel electrodes, and the potential difference ( $\Delta E_{a,c}$ ) between the anodic ( $E_a$ ) and cathodic ( $E_c$ ) peak potentials is a measure of the reversibility of the redox reaction [26,27]. Anodic peak potential ( $E_{pa}$ ) and cathodic peak potential ( $E_{pc}$ ) are found to decrease after the doping of MgO. Compared with that of pure  $\beta$ -Ni(OH)<sub>2</sub>, the  $\Delta E$  values of the MgO added  $\beta$ -Ni(OH)<sub>2</sub> are decreased, which indicates that the addition of MgO is found to improve the reversibility of the electrode reaction remarkably.

Table 1. Potential values of CV features for pure  $\beta$ -Ni(OH)<sub>2</sub> and MgO substituted  $\beta$ -Ni(OH)<sub>2</sub> electrode materials.

Sample	$E_a$ (V)	$E_c$ (V)	$E_{OE}$	$\Delta E_{a,c}$ (V)	$E_{OE} - E_a$ (V)
Pure $\beta$ -Ni(OH) <sub>2</sub>	0.393	0.155	0.455	0.238	0.062
MgO substituted $\beta$ -Ni(OH) <sub>2</sub>	0.334	0.101	0.460	0.233	0.126

The strong increase in the current at the end of anodic peak sweep is due to the oxygen evolution reaction (Eq. 4):



The polarized current is low before the appearance of electrochemical reaction because there are not any free electrons in the electrolyte. The presence of polarized current indicates the occurrence of redox reaction. As shown in the Fig. 6, the strong terminal peak deals with the oxidation peaks of water. When nickel hydroxide electrode is being charged, oxygen evolution reaction is a parasitic side reaction, which has negative effects on the charge efficiency and the structure of the electrode. Compared with that of pure  $\beta$ -Ni(OH)<sub>2</sub>, the ( $E_{OE} - E_{pa}$ ) values of the MgO added  $\beta$ -Ni(OH)<sub>2</sub> are increased, which indicates that the addition of MgO is found to increase the separation of the oxidation current peak of the active material from the oxygen evolution current[25].

In Fig. 7 cyclic voltammograms of electrodes with pure  $\beta$ -Ni(OH)<sub>2</sub> and MgO added  $\beta$ -Ni(OH)<sub>2</sub> electrode materials at different scan rates are presented. The shape of the curve indicates that the observed capacitance characteristic is distinct from that of the electric double layer capacitor, which would produce a CV curve that is usually close to an ideal rectangular shape. It can be seen from Fig. 7 that the shape of CV curves of the  $\beta$ -Ni(OH)<sub>2</sub> and electrode with MgO additive is not significantly influenced by the increasing of the scan rates. This indicates the improved mass transportation and electron conduction within the material. Further, it is well-known that the electrochemical reaction process of a nickel hydroxide electrode is limited by proton diffusion through the lattice [45-47]. According to the Randles - Sevcik equation [45], at 25 °C the peak current,  $i_p$ , in the cyclic voltammogram can be expressed as

$$i_p = 2.69 \times 10^5 \times n^{\frac{3}{2}} \times A \times D^{\frac{1}{2}} \times C_o \times v^{\frac{1}{2}} \quad (5)$$

where  $n$  is the electron number of the reaction (~1 for  $\beta$ -Ni(OH)<sub>2</sub>),  $A$  is the surface area of the electrode (1 cm<sup>2</sup>),  $D$  is the diffusion coefficient,  $v$  is the scanning rate, and  $C_o$  is the initial concentration of the reactant. For Ni(OH)<sub>2</sub> electrode,  $C_o = \rho/M$ , where  $\rho$  and  $M$  are the density (4.1 g/cm<sup>3</sup>) and the molar mass (92.7 g/mol) of Ni(OH)<sub>2</sub> respectively.

Fig. 8 displays the relationship between the anodic peak current ( $i_p$ ) and the square root of the scan rate ( $v^{1/2}$ ) for both electrodes. The linear relationship between  $i_p$  and  $v^{1/2}$  confirms that the electrode reaction of  $\beta$ -Ni(OH)<sub>2</sub> is controlled by proton diffusion. Using the slope of the fitted line in Fig. 8 and Equation (5), the proton diffusion coefficient ( $D$ ) for pure  $\beta$ -Ni(OH)<sub>2</sub> electrode material is calculated to be,  $D = 1.44 \times 10^{-12}$  cm<sup>2</sup> sec<sup>-1</sup>, which is comparatively smaller than that of MgO added  $\beta$ -Ni(OH)<sub>2</sub> electrode material with  $D = 7.3425 \times 10^{-12}$  cm<sup>2</sup> sec<sup>-1</sup>. Thus, the proton diffusion coefficient was found to increase with the addition of MgO in to  $\beta$ -Ni(OH)<sub>2</sub> electrode material. Observed higher proton diffusion coefficient in the present MgO added  $\beta$ -Ni(OH)<sub>2</sub> electrode is attributable to fewer intercalated anions, water molecules adsorbed on the surface of the  $\beta$ -Ni(OH)<sub>2</sub> particles and high structural disorder density. The high density of structural disorder for nickel hydroxide powder is beneficial for the acceleration of solid-state proton diffusion in the Ni(OH)<sub>2</sub> lattice and will diminish the

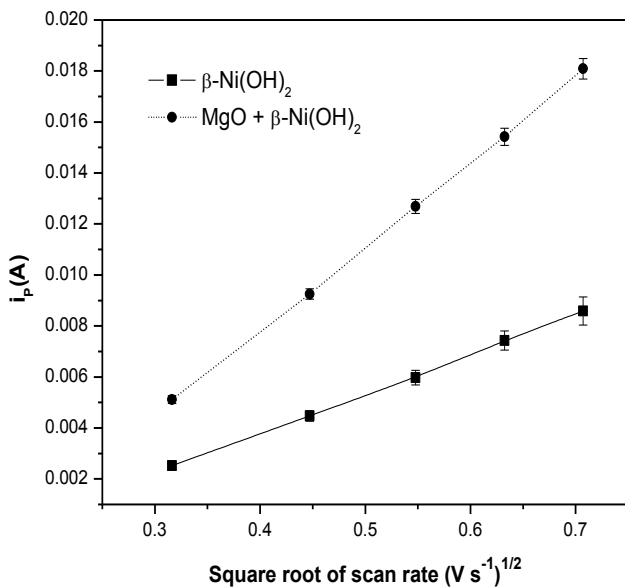


Figure 8. Relationship between the anodic peak current ( $i_p$ ) and the square root of the scan rate ( $v^{1/2}$ ) for pure  $\beta\text{-Ni(OH)}_2$  electrode and MgO added  $\beta\text{-Ni(OH)}_2$  electrode.

concentration polarization of protons during charge and discharge, leading to better charge-discharge cycling behavior [43].

#### 4. CONCLUSIONS

$\beta$ -nickel hydroxide ( $\beta\text{-Ni(OH)}_2$ ) was successfully synthesized using precipitation method. The effects of MgO additive on the structure and electrochemical performance of  $\beta\text{-Ni(OH)}_2$  electrode are examined. FT-IR and XRD analyses showed that the prepared  $\text{Ni(OH)}_2$  was a pure  $\beta$  phase. The results of the FTIR spectroscopy and TG-DTA studies indicate that the MgO added  $\beta\text{-Ni(OH)}_2$  contains water molecules and anions. SEM image indicated that the  $\beta\text{-Ni(OH)}_2$  electrode material is flaky and appears as aggregates of irregular tabular shapes, CV curves showed a pair of strong redox peaks as a result of the Faradaic redox reactions of  $\beta\text{-Ni(OH)}_2$  particles. Anodic peak potential ( $E_{pa}$ ) and cathodic peak potential ( $E_{pc}$ ) values are found to decrease remarkably after the incorporation of MgO into the  $\beta\text{-Ni(OH)}_2$  electrode. Further, addition of MgO is found to improve the reversibility of the electrode reaction remarkably. Compared with  $\beta\text{-Ni(OH)}_2$  electrode, MgO added  $\beta\text{-Ni(OH)}_2$  electrode is found to exhibit higher proton diffusion coefficient. These findings suggest that the MgO added  $\beta\text{-Ni(OH)}_2$  electrode possess improved electrochemical properties such as enhanced reversibility of electrode reaction and higher proton diffusion coefficient and thus can be recognized as a promising candidate for the battery electrode applications.

#### 5. ACKNOWLEDGEMENTS

Authors wish to acknowledge the Sophisticated Test and Instrumentation Centre (STIC), CUSAT, Cochin for TG-DTA analysis.

#### REFERENCES

- [1] Lin Li, Zhong Wu, Shuang Yuan, Xin-Bo Zhang, Energy Environ. Sci., 7, 2101 (2014).
- [2] Zhong Wu, Xiao-Lei Huang, Zhong-Li Wang, Ji-Jing Xu, Heng-Guo Wang, Xin-Bo Zhang, Sci. Rep., 4, 3669 (2014).
- [3] Zhong-Li Wang, Dan Xu, Ji-Jing Xu, Xin-Bo Zhang, Chem. Soc. Rev., 43, 7746 (2014).
- [4] H. Bode, K. Dehmelt, J. Wittle, Electrochim. Acta, 11, 1079 (1966).
- [5] S.U. Folk, A.J. Salkind, Alkaline Storage Batteries, John Wiley & Sons, New York (1969).
- [6] H.S. Lim, S.A. Verzwyvelt, J. Power Sources, 62, 41 (1996).
- [7] D.E. Reisner, A.J. Salkind, P.R. Strutt, T.D. Xiao, J. Power Sources, 65, 231 (1997).
- [8] S. Nathira Begum, V.S. Muralidharan, C. Ahmed Basha, Int. J. Hydrogen energy, 34, 1548 (2009).
- [9] T. Pan, J.M. Wang, Y.L. Zhao, H. Chen, H.M. Xiao, J.Q. Zhang, Mater. Chem. Phys., 78, 711 (2003).
- [10] P. Xu, X.J. Han, B. Zhang, Z.S. Lv, X.R. Liu, J. Alloys Compd., 436, 369 (2007).
- [11] M. Vidotti, R.P. Salvador, S.I.C. Torresi, Ultrason. Sonochem., 16, 35 (2009).
- [12] P. Oliva, J. Leonardi, J.F. Laurent, C. Delmas, J.J. Braconnier, M. Figlarz, J. Power Sources, 8, 229 (1982).
- [13] R.D. Armstrong, G.W.D. Briggs, E.A. Charles, J. Appl. Electrochem., 18, 215 (1988).
- [14] K. Watanabe, M. Koseki, N. Kumagai, J. Power Sources, 58, 23 (1996).
- [15] L. Guerlou-Demourgues, C. Delmas, J. Electrochem. Soc., 143, 561 (1996).
- [16] D. Yunchang, Y. Jiongliang, C. Zhaorong, J. Power Sources, 69, 47 (1997).
- [17] A.K. Sood, J. Appl. Electrochem. 16, 274 (1986).
- [18] C. Chakkaravarthy, P. Periasamy, S. Jegannathan, K.I. Vasu, J. Power Sources, 35, 21 (1991).
- [19] D.M. Constantin, E.M. Rus, L. Oniciu, L. Ghergari, J. Power Sources, 74, 188 (1998).
- [20] Li Jun, Li Rong, Wu Jianming, Su Hang, J. Power Sources, 79, 86 (1999).
- [21] S. Kulcsar, J. Agh, A. Fazekas, J. Vigh, Z. Bujdos, J. Power Sources, 8, 55 (1982).
- [22] W. Xiayou, L. Hean, Y. Hongping, P.J. Sebastian, S.A. Gamboa, Int. J. Hydrogen Energy, 29, 967 (2004).
- [23] Changjiu Liu, Yanwei Li, J. Alloys and Compd., 478, 415 (2009).
- [24] P. Baraldi, G. Davolio, Mater. Chem. Phys., 21, 143 (1989).
- [25] L. Petersen Steven, E. Tallman Dennis, Analytical Chemistry, 62, 459 (1990).
- [26] W.G. Zhang, W.Q. Jiang, L.M. Yu, Z.Z. Fu, W. Xia, M.L. Yang, Int. J. Hydrogen Energy, 34, 473 (2009).
- [27] B. Liu, H. Yuan, Y. Zhang, Z. Zhou, D. Song, J. Power Sources, 79, 277 (1999).
- [28] B. Shruthi, V. Bheema Raju, B.J. Madhu, Spectrochimica Acta

- Part A, 135, 683 (2015).
- [29]A. Audemer, A. Delahaye, R. Farhi, N. Sac-Epee, J. M. Tarascon, *J. Electrochem. Soc.*, 144, 2614 (1997).
- [30]Ding Yunchang, Yuan Jiong Liang, Li Hui, Chang Zhaorong, Wang Zeyun, *J. Power Sources*, 56(2), 201 (1995).
- [31]Subramanian V, Boovaragavan V, Potukuchi K, Diwakar V, Guduru A., *Electrochem. Solid State Lett.*, 10(2), A25 (2007).
- [32]Mustafa Aghazadeh, Ahmad Nozad Golikand, Mehdi Ghaemi, *Int. J. Hydrogen energy*, 36, 8674 (2011).
- [33]M. Oshitani, Y. Sasaki, K. Takashima, *J. Power Sources*, 12, 219 (1984).
- [34]P. Baraldi, G. Davolio, G. Fabbri, T. Manfredini, *Mater. Chem. Phys.*, 21, 479 (1989).
- [35]T.N. Ramesh, P.V. Kamath, *Bull. Mater. Sci.*, 31, 169 (2008).
- [36]Z.H. Liang, Y.J. Zhu, X.L. Hu, *J. Phys. Chem. B*, 108, 3488 (2004).
- [37]W.K. Hu, X.P. Gao, D. Noreus, T. Burchardt, N. Nakstad, *J. Power Sources*, 160, 704 (2006).
- [38]B.C. Cornilsen, P.J. Karjala, P.L. Loyselle, *J. Power Sources*, 22, 351 (1988).
- [39]Y.L. Zhao, J.M. Wang, H. Chen, T. Pan, J.Q. Zhang, C.N. Cao, *Int. J. Hydrogen Energy*, 29, 889 (2004).
- [40]H. Zhang, H. Liu, X. Cao, S. Li, C. Sun, *Mater. Chem. Phys.*, 79, 37 (2003).
- [41]H. Chen, J.M. Wang, T. Pan, H.M. Xiao, J.Q. Zhang, C.N. Cao, *Int. J. Hydrogen Energy*, 28, 119 (2003).
- [42]J. Chen J, D.H. Bradhurst, S. Dou, H. Liu, *J. Electrochem. Soc.*, 146, 3606 (1999).
- [43]Q.S. Song, C.H. Chiu, S.L.I. Chan, *Electrochim. Acta*, 51, 6548 (2006).
- [44]Q.S. Song, C.H. Chiu, S.L.I. Chan, *J. Solid State Electrochem.*, 12, 133 (2008).
- [45]A.H. Zimmerman, P.K. Effa, *J. Electrochem. Soc.*, 131(4), 709 (1984).
- [46]X. Cao, J. Wei , Y. Luo, Z. Zhou, Y. Zhang, *Int. J. Hydrogen Energy*, 25(7), 643 (2000).
- [47]Enbo Shangguan, Zhaorong Chang, Hongwei Tang, Xiao-Zi Yuan, Haijiang Wang, *Int. J. Hydrogen Energy*, 35, 9716 (2010).